

Behaviour of porous aerostatic bearings with various restrictor permeabilities

Maria Hübner², Mikael Miettinen¹, Valtteri Vainio¹, Christian Cierpka², René Theska², Raine Viitala¹

¹Aalto University, ²TU Ilmenau

maria.huebner@tu-ilmenau.de

Abstract

Aerostatic bearings are externally pressurized gas lubricated bearings. Aerostatic bearings are used in high speed and precision motion applications due to low friction and high accuracy. They use a restrictor to limit the flow of the gas into the bearing gap. The presence of the restrictor increases the stability of the bearing against self-excited vibrations. This study focuses on porous graphite restrictors and the effect of permeability on the behaviour of the bearing.

The bearings were studied both experimentally and with a simulation model. Flat bearing pads with 37 mm diameter and different restrictor bulk permeability were manufactured and tested.

Experimental measurements were conducted on a test setup allowing loading of the bearing against a ground steel plate. The load was supplied with a series of weights. The air gap was measured with a linear length gauge, measuring the displacement of the air bearing. The pressure was controlled with a regulator and the flow rate into the bearing was measured.

In order to build an accurate simulation model, the permeability of the used material was calculated from the measured short circuit flow through each 4.5 mm thick sample. The flow in the porous material and in the restrictive layer follows Darcy's law, the flow in the air gap is described by the Navier-Stokes-equation. The simulation model was validated with experimental results.

Measurement and simulation results include the air gap height, load and flow rate at a supply pressure of 0.4 MPa. According to previous research and preliminary results the surface restrictor layer has increased the resistance of the bearing to self-excited air-hammer vibration, leading to a higher load capacity.

Aerostatic bearing, porous restrictor, restrictive layer

1. Introduction

Aerostatic bearings are commonly used in precision motion and positioning applications. Aerostatic bearings have low friction, high positioning accuracy, no stick-slip phenomenon and tolerate high operating speeds. However, the bearings have a relatively low load capacity. The bearing is lubricated by externally pressurized gas that is fed into the bearing gap through a restrictor. A restrictor restricts the flow of the air entering the bearing gap and improves the stiffness of the bearing and reduces the air consumption. Common restrictor types include orifices, grooves, slots and porous materials.

Aerostatic bearings with porous restrictors are preferred to orifice-fed bearings as they offer higher load capacity and high stiffness over a large range of air gap height as shown by, for example, Fourka and Bonis [1].

Different studies to determine the design parameters affecting the performance of porous aerostatic bearings have been made [1-9] and were reviewed by Gao et al. [10].

One parameter that influences load capacity and stiffness is the permeability of the porous material. Fourka and Bonis found that the permeability has to be smaller than 10^{-12} m² to achieve a good performance. They performed an in-silico study of permeability in different orders of magnitude, in order to get a basic understanding of the influence of the permeability. [1]

In this paper, three in-house manufactured porous bearings from commercially available graphite materials and one commercially available porous bearing were investigated. The results were used to validate a simulation model, which enables further parameter studies.

2. Methods

The structure of the investigated bearing is shown in Figure 1, and the dimensions shown are explained in Table 1. The bearing consists of an aluminium body and the porous restrictor, and the commercially available bearing has an additional restrictive layer. The external pressure supply distributes the inlet air to the porous restrictor through the inlet grooves. The air flows into the bearing gap through the porous restrictor and flows out of the gap to the ambient atmosphere.

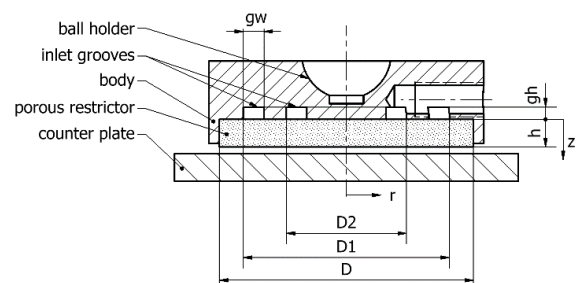


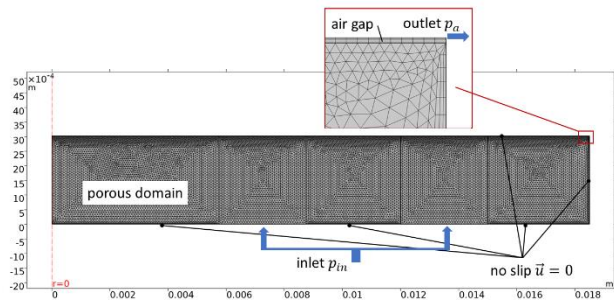
Figure 1. Cross-section of the investigated bearing.

The bearing was investigated numerically and experimentally with the focus on the static stiffness and load capacity to develop a robust simulation model with a good understanding of the influence of the permeability.

Table 1. Dimensions of the investigated bearing.

Dimension	Description	Value (mm)
D	Diameter of porous restrictor	37.0
D1	Outer diameter of outer groove	30.0
D2	Outer diameter of inner groove	17.5
h	Height of porous restrictor	4.5
gh	Height of groove	1.8
gw	Width of groove	3.0

In the numerical simulation, the air gap was set between 1 and 25 μm . The load was calculated with the resulting pressure distribution in the air gap at the counter plate and the volume flow was calculated with the velocity profile at the edge of the bearing. On the contrary, the experimental measurements were conducted with a set load between 6 and 360 N and the resulting air gap and volume flow at the inlet were measured.

**Figure 2.** 2D simulation model of porous bearing.

2.1 Simulation model

The simulation model for the bearing consists of the porous domain in the restrictor of the bearing and the air gap between the bearing and the counter plate as shown in Figure 2.

The flow through a porous material is defined by the pressure loss $\frac{\partial p}{\partial z}$ and is described by Darcy's law as stated in eq. (1)

$$\vec{v} = -\frac{K}{\eta} \frac{\partial p}{\partial z} \quad (1)$$

with the velocity of the fluid \vec{v} , the dynamic viscosity of the fluid η and the specific permeability K . The latter one is independent of the fluid properties but depends on the geometry of the porous material. In the case of a single-phase flow the specific permeability equals the permeability κ of the porous material.

In the case of a laminar flow with non-linear drag coefficient, which can be assumed with a Reynolds number in the range of 1-10, eq. (1) is extended by the Forchheimer equation:

$$\frac{\partial p}{\partial z} = -\frac{\eta}{K} \vec{v} - c_F \kappa^{-\frac{1}{2}} \rho_f |\vec{v}| \vec{v} \quad (2)$$

$$c_F = \frac{1.75}{\sqrt{150}} \cdot \varepsilon_p^{-3/2} \quad (3)$$

with the density of the fluid ρ_f and the Forchheimer coefficient c_F , shown in eq. (3). Latter depends on the porosity ε_p of the restrictor. [11]

The flow in the air gap is described by the Navier-Stokes equation for the stationary case without additional forces:

$$\rho_f \vec{v} \cdot (\nabla \vec{v}) = -\nabla p + \eta (\nabla^2 \vec{v}) \quad (4)$$

In this study, the commercial software COMSOL 5.4 with the 'free and porous media flow' interface was used. It is based on the finite element method. The simulation model is 2D axis-symmetric to reduce computational requirements. The mesh was studied in a refinement study. The resulting mesh consists of 5 layers in the z-direction of rectangular elements in the air gap and of a free triangular mesh with the setting 'finer for fluid

dynamics' in the porous domain. This results in a total amount of 751290 elements.

The following assumptions and boundary conditions were used in the simulation:

- Air as fluid at isothermal conditions, $T_\infty = 20 \text{ }^\circ\text{C}$
- Gravitational forces neglectable
- Weakly compressible flow (Mach number $Ma = \frac{v}{c} < 0.3$)
- Laminar flow (Reynolds number $Re = \frac{\rho_f v D_{char}}{\eta} < 10$)
- Pressure-driven flow, with inlet pressure $\Delta p = p_{in,abs} - p_a = 0.4 \text{ MPa}$ and ambient pressure $p_a = 0.1 \text{ MPa}$
- No-slip-boundary-condition at all outer walls and the counter plate
- Interface between porous domain and free flow has continuous pressure and velocity fields, which implies a stress discontinuity [12]

2.2 Measurement setup

The measurement setup, shown in Figure 3, loaded the investigated bearings (see Table 2) against a ground steel plate. The setup allowed measurement of the gap height, air consumption and load capacity of the investigated bearings. The bearing was loaded using a series of weights and the amount was changed to vary the load.

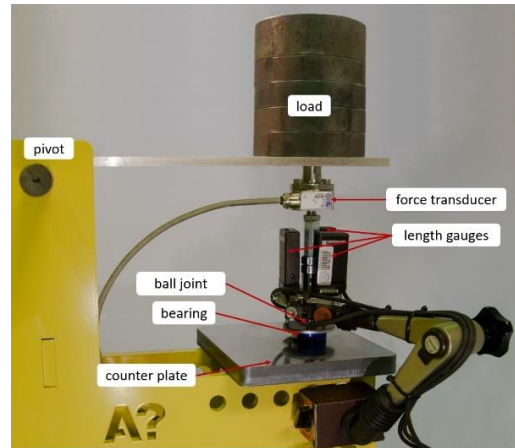
**Figure 3.** The measurement setup.

Table 2. Three of the four investigated bearings were manufactured in house. The dimensions of the in-house bearings match the dimensions of the commercial bearing. The graphite restrictor was mounted to the aluminium housing with an epoxy resin. The surface of the bearing was lapped with 6-micron abrasive film.

Bearing	Graphite material
1	AXM-5Q, POCO Material (USA)
2	TM1, POCO Material (USA)
3	Q70, Meusburger Georg GmbH & Co KG (Austria)
4	commercially available bearing S104001 from New Way Bearings (USA)

The measurement setup used a NI USB-6215 DAQ device to control the pressure regulators and record the measurements. The air consumption was measured with a SMC PFM510 flow meter at the inlet, the load capacity was measured with a HBM U2B force transducer and AE 101 amplifier, and the gap height between the bearing and the counter plate was measured with three Heidenhain MT-12 length gauges. The range and accuracy of each measurement device can be found in Table 3.

Three length gauges were used to neglect the effect of the bearing tilting during the measurement. The displacement of the three gauges was averaged and compared against the reference measurement with the bearing air supply turned off.

Table 3. Range and accuracy of measurement devices.

Device	Range	Accuracy
NI USB-6215	-10 – 10 V	$\pm 2.690 \mu\text{V}$
SMC PFM510	0.2 – 10 l/min	$\pm 3 \%$ F.S.
HBM U2B (5kN)	Calibrated for 600 N	$\pm 1 \%$ F.S.
HBM AE 101	-10 – 10 V	$\pm 1 \%$ F.S.
Heidenhain MT-12	12 mm	$\pm 0.5 \mu\text{m}$

Each bearing was measured 5 times to investigate the repeatability of the measurement and the standard uncertainty $u(\bar{x})$ of type A was calculated.

The measurements were carried out with the following procedure:

1. The investigated bearing was placed on the steel plate and the loading arm was put in place.
2. The displacement of the bearing was measured to set the reference point for the air gap measurement.
3. All weights were placed on top of the bearing.
4. The load was decreased in steps and the displacement and air consumption was measured at each step.
5. After measurements, the air supply was turned off and the next bearing sample could be measured, starting from step 1.

2.3 Data processing

To calculate the static stiffness S , the graphs of the load capacity F over the air gap height h were derived with

$$S = \frac{\partial F}{\partial h}. \quad (5)$$

The permeability κ was determined with eq. (6) from the measured short circuit flow Q . The short circuit flow is the free flow into the ambient atmosphere, measured at the desired supply pressure.

$$\kappa = \frac{8 \cdot Q \cdot \eta \cdot h \cdot p_a}{\pi \cdot D_e^2 \cdot (p_{in,abs}^2 - p_a^2)}, \quad (6)$$

where h is the thickness of the porous material, p_a is the absolute ambient pressure and $p_{in,abs}$ is the absolute supply pressure. The measured permeability was used in the simulation model. For the case of bearing 4 with an additional restrictor layer this reduces the two different permeabilities to one value. This was addressed in a separate model with two porous domains, for which the bulk permeability was measured separately and the resulting permeability in the restrictive layer was calculated.

3. Results

The presented preliminary results were measured at a relative bearing supply pressure of 0.4 MPa.

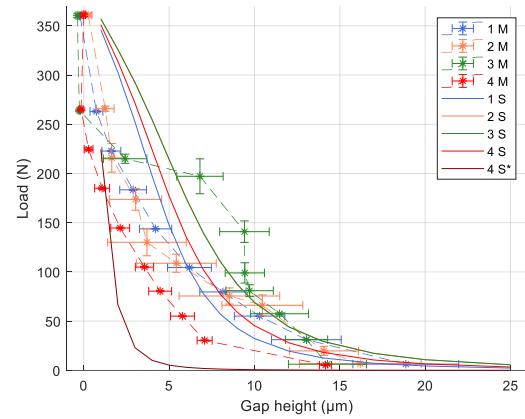
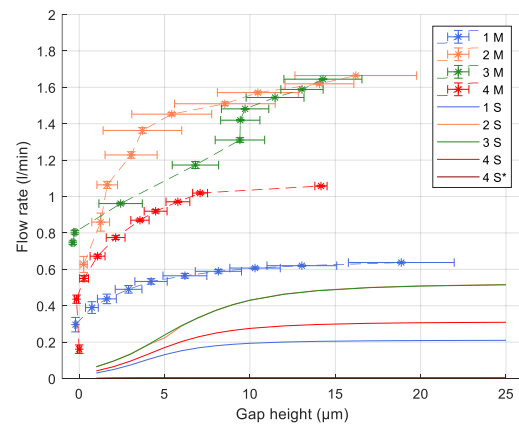
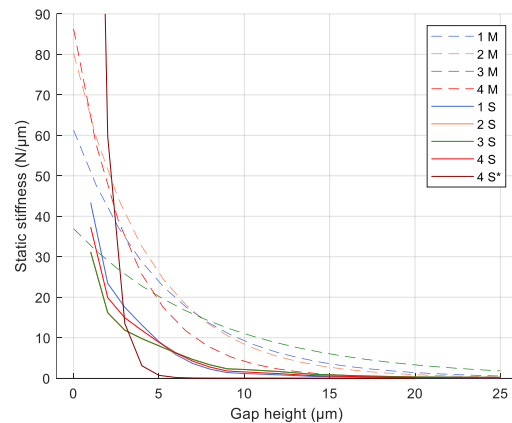
The permeability of the graphite restrictor in each bearing was determined with the measurement of the short circuit flow. The permeabilities, calculated using eq. (6), are presented in Table 4.

Table 4. Permeability of the investigated bearings. Bearings 1-3 are manufactured in-house and bearing 4 is a commercially available bearing, the porosity for it is calculated.

Bearing	h (mm)	Porosity (%)	Permeability at 0.4 MPa (m ²)
1	4.49	0.23	$(0.710 \pm 0.0515) \cdot 10^{-15}$
2	4.43	0.2	$(1.768 \pm 0.1283) \cdot 10^{-15}$
3	4.48	0.2	$(1.764 \pm 0.1279) \cdot 10^{-15}$
4	4.50	0.33	$(1.052 \pm 0.1279) \cdot 10^{-15}$

The load capacities of the investigated bearing are presented in Figure 4, and the volumetric flow rates at corresponding gap heights are presented in Figure 5.

The static stiffness of the bearing, which was calculated using eq. (5), is presented in Figure 6.

**Figure 4.** Load capacity in relation to the gap height at 0.4 MPa bearing supply pressure. Measurement points are marked with stars and dashed lines. Solid lines depict the simulated results. Graph 2S is hidden behind 3S. Error bars represent the standard uncertainty of the measurement. The abbreviations in the legend stand for M – measured, S – simulated and S* - simulated with restrictive layer.**Figure 5.** Volume flow in relation to the gap height. Measurement points are marked with stars and dashed lines. Solid lines depict the simulated results. Graph 2S is hidden behind 3S. Error bars represent the standard uncertainty of the measurement. The abbreviations in the legend stand for M – measured, S – simulated and S* - simulated with restrictive layer.**Figure 6.** Static Stiffness in relation to the gap height. Dashed line is used for measurement results and solid line is used for simulation results. Graph 2S is hidden behind 3S. The abbreviations in the legend stand for M – measured, S – simulated and S* - simulated with restrictive layer.

4. Discussion

The present study compares the performance of aerostatic bearings with various restrictor permeabilities.

The measured load agrees fairly well to the simulated load for bearings 1, 2 and 4 (Figure 4). During the measurements of bearing 2 and 3, audible vibrations occurred. The vibration was presumably the self-excited air-hammer phenomena [13]. The increased uncertainty of the measurements of those bearings, shown by the uncertainty bars in Fig. 4 and 5, is an effect of the vibration.

The results in Figure 6 suggest, that the stiffness of the bearings increases significantly at low air gap height or that the bearing contacts the counter plate at high loads. This occurs at 350 N and 260 N, for the bearings 1 & 2 and 3 & 4, respectively. The experimentally determined stiffness of bearings 1-3 approaches the same value from 10 μm onwards, whereas bearing 4 has a larger curvature and agrees better with the numerical data.

In Figure 5, the measured flow rates are larger than the simulated by a factor of 3. Presumably the difference originates from some error in the simulation, as the measured values correspond to the ones provided by the manufacturer of the commercial bearing. Possible error sources are the calculation of the permeability, leakage of the real bearing or the assumption of weakly compressible flow. Further investigation will be carried out to determine the concrete influences.

The commercially available bearing, denoted with number 4, has an added surface restrictor layer, while the in-house made bearings have none. The simulation model with the surface layer is closer to the measured results than the model without the surface layer.

The comparison regarding the permeability of the bearings is difficult, as the measurement uncertainties are high in comparison to the differences between the load capacity. It can be seen that the volume flow rate highly depends on the permeability, with an increase of the volume flow rate with increasing permeability.

The measurement setup produced systematic uncertainties to the measurement results. These uncertainties were due to e.g. the insufficient stiffness of the counter plate, resulting in a deflection in the range of a few micrometres under the measurement load. The negative gap heights visible in the results are presumably a result of the measurement setup deforming or due to movement of the bearing. Additionally, the ball joint introduces a moment to the bearing, as the friction in the joint increases as the load on the bearing increases.

5. Conclusion

The present study investigated the effect of the restrictor permeability on the load capacity, gap height, and air consumption of porous aerostatic bearings with 37 mm diameter. Three custom bearings with varying restrictor permeability and one commercially available bearing were compared.

The investigation consisted of an experimental study and a numerical simulation based on the measured permeability of the bearings.

The compared parameters include the load capacity, volume flow rate and static stiffness of the bearing. It was shown that there are some differences between the numerical and the experimental results especially in the volume flow rate, but the qualitative behaviour is visible for both approaches.

Due to occurring vibrations in the measurement of bearing 2 and 3, a proportional relation between the permeability and the measured load or volume flow can only be assumed from the

exponential fit. Based on the numerical curves and the fit of the experimental data, it is possible to assume a proportional increase of the load capacity as well as the volume flow with increasing permeability.

To achieve a better agreement between the numerical and the experimental results, the assumptions for the numerical calculations must be reviewed. As the numerical solution is based on perfect surface qualities, dimensions and measurements, it increases the disagreement between numerical and experimental results. If possible, surface roughness of both counter plate and bearing should be included in the model, as well as measured in the experimental setup.

Further studies should focus on the effect of manufacturing errors on the performance of the bearing and to decrease the uncertainties of the measurements by improving the measurement setup.

The following improvements could reduce the measurement uncertainties:

- Replacing the pivot by a flexure and thus eliminating friction from the system.
- Replacing the ball joint with a flexure to enable angular and tilting movement without friction.
- Increasing the stiffness of the measurement frame and the counter plate to avoid deflection in the measurement path.
- Polished surface with high surface quality for the counter plate for accurate measurement of the air gap height.

References

- [1] Fourka M and Bonis M, *Wear* **210** 311-317
- [2] Cui C and Ono K, 1997 *Transactions of the ASME* **119** 486-492
- [3] Gururajan K and Prakash J, 1999 *Transactions of the ASME* **121** 139-147
- [4] Yoshimoto S and Kohno K, 2001 *Journal of Tribology* **123.3** 501-508
- [5] Schenk C, 2007 *Dissertation Technische Universität Ilmenau* (in german)
- [6] Otsu Y, Miyatake M, Yoshimoto S, 2011 *Journal of Tribology* **133** 011701-1 - 10
- [7] Huang T, Hsu S, Wang B and Lin S, 2014 *Key Engineering Materials* **625** 384-391
- [8] Heidler N, 2015 *Dissertation Universitätsverlag Ilmenau* (in german)
- [9] Cui H, Wang Y, Yue, X, Huan M and Wei Wang, 2017 *Tribology International* **115** 246-260
- [10] Gao Q, Chen W, Lu L and Cheng K, 2019 *Tribology International* **135** 1-17
- [11] Nield D A and Bejan A, 2017 *Springer International Publishing*, 1-19
- [12] Bars M L and Worster M G, 2006 *J. Fluid Mechanics* **550** 149-173
- [13] Jacob J S, Yu J J, Bently D E and Goldman P, 2001 *Int. Symp. on Stability Control of Rotating Machinery*